![sciendo]

MULTI-METHOD LUMINESCENCE DATING OF OLD FLUVIAL SEDIMENTS FROM NORTHERN TIAN SHAN, CHINA

KECHANG LI[1, 2, 4], JINTANG QIN[1, 4], JIE CHEN[1, 4], JUN SHEN[2] and SHENG-HUA LI[3]

[1]*State Key Laboratory of Earthquake Dynamics, Institute of Geology, China Earthquake Administration, Beijing, China*
[2]*Research Centre for Disaster Mitigation, Institute of Disaster Prevention, Langfang, Hebei, China*
[3]*Department of Earth Sciences, The University of Hong Kong, Hong Kong, China*
[4]*Xinjiang Pamir Intracontinental Subduction National Field Observation and Research Station, Beijing, China*

Abstract: At the eastern tip of Anjihai anticline on the northern piedmont of Tian Shan (northwest China), deformed fluvial deposits have recorded active folding since the Pleistocene, but the absence of accurate ages makes it difficult to evaluate the anticline's shortening rate. Geological studies ascribed the fluvial strata to the early Pleistocene, which poses potential challenges for luminescence dating. In this study, multi-methods luminescence dating was applied to a fluvial sand sample taken from the sandy bed of the deformed basal strata. Single grain post-Infrared Infrared Stimulated Luminescence (pIRIR) and multiple-aliquot-regenerative (MAR) dose along with multiple-elevated-temperature pIRIR (MET-pIRIR) procedures were applied to determine the paleodose of the sample. The methodological uncertainties, such as thermal transfer and initial sensitivity change, were treated by increasing the test dose and performing dose recovery test. With consideration of the potential partial bleaching and anomalous fading, various statistical metrics were applied to the D_e values determined by using the single grain $pIRIR_{225}$, single grain $pIRIR_{290}$ and MAR-MET-$pIRIR_{290}$ signals. The minimum age model (MAM) D_e values are 11% – 17% lower than the central age model (CAM) D_e values in general, and the MAM D_e values determined by the single grain pIRIR procedures are underestimated by more than 40% when compared with those determined by MAR-MET-$pIRIR_{290}$ procedure. The MAM MAR-MET-$pIRIR_{290}$ D_e of 811 ± 44 Gy results in a burial age of 284 ka for the basal deformed fluvial strata, which is much younger than the proposed early Pleistocene age.

Keywords: Fluvial sediment, K-feldspar, optical dating, MAR-MET-pIRIR, Tian Shan.

1. INTRODUCTION

A thrust-and-fold belt is located on the northern piedmont of Chinese Tianshan Mountain, and it is featured by rows of emerging fault-related folds with the west-east strike (Avouac *et al.*, 1993; Deng *et al.*, 2000). One of these folds is the Anjihai anticline, which is located on the most northern deforming front (**Fig. 1a**). The

Corresponding author: J. Qin
e-mail: jtqin@ies.ac.cn

sandy bed (**Fig. 1b**) at the bottom of the outcrop on its eastern tip of Anjihai anticline is supposed to be early Pleistocene fluvial sediments and is southward tilted by 5° (Deng *et al.*, 2000, 2013). Since the Jingou River, which cuts across the Anjihai anticline, flows northward, the observed tilting to the south would be attributed to the rotation of the sandy bed due to anticline growth. Therefore, the angle of such a rotation is 5° at least. However, it is a lack of depositional ages for the sandy bed. If the depositional age is determined, the pattern and rate of anticline growth could be constrained in combination with the rotation angle (Li *et al.*, 2013b). Such constraints are critical for evaluating the seismic hazard of the cities nearby since the deformation rate would be higher than previously thought if its depositional age is not as old as early Pleistocene.

Luminescence dating technique is of potential to constrain the depositional age of these deformed strata. The post-Infrared Infrared Stimulated Luminescence (post-IRIRSL) signals of potassium feldspars (K-feldspar) are achieved either in two steps (pIRIR, Thomsen *et al.*, 2008; Buylaert *et al.*, 2009; Thiel *et al.*, 2011) or in multiple steps (MET-pIRIR, Li and Li, 2011). These procedures help extend the upper limit of luminescence dating to 300 ka to 500 ka on aeolian loess (Li and Li, 2012; Chen *et al.*, 2015), for which the post-IR IRSL signals were bleached to a negligible level (Buylaert *et al.*, 2011; Li *et al.*, 2014). However, the incomplete bleaching of post-IR IRSL signals prior to deposition due to their slow

bleaching characteristics complicates its application to dating fluvial and other water-lain sediments (e.g., Kars *et al.*, 2014; Colarossi *et al.*, 2015).

It was reported that the small aliquot K-feldspar MET-pIRIR ages were overestimated by 50% for a Holocene fluvial sample from Northern Tianshan (Fu *et al.*, 2015). As a potential way to tackle the partial bleaching problem, single grain procedure is increasingly employed for dating water-lain sediments by incorporating various pIRIR signals (Nian *et al.*, 2012; Reimann *et al.*, 2012; Brown *et al.*, 2015; Rhodes, 2015; Brill *et al.*, 2018; Malatesta *et al.*, 2018; Li *et al.*, 2018; Rui *et al.*, 2019). For fluvial samples older than 10 ka, the high-temperature pIRIR signals, e.g., $pIRIR_{225}$ and $pIRIR_{290}$ signals, are employed. With consideration of the bleaching rate, the $pIRIR_{225}$ signal is more frequently employed in recent studies of fluvial samples (Brown *et al.*, 2015; Rhodes, 2015; Brill *et al.*, 2018; Malatesta *et al.*, 2018). Rhodes (2015) showed that the single grain K-feldspar $pIRIR_{225}$ ages are consistent with the independent ages ranging from 1 ka to 100 ka. However, the intrinsically old property of the strata leads to complexities for single grain dating. Firstly, the anomalous fading of pIRIR signals would be considerable even at high stimulation temperature (Kolb and Fuchs, 2018; Malatesta *et al.*, 2018), but its rates are difficult to measure and rather variable amongst grains (Reimann *et al.*, 2012; Rhodes, 2015; Smedley *et al.*, 2015). Secondly, the upper dating limit of single grain K-feldspar pIRIR procedure might be around
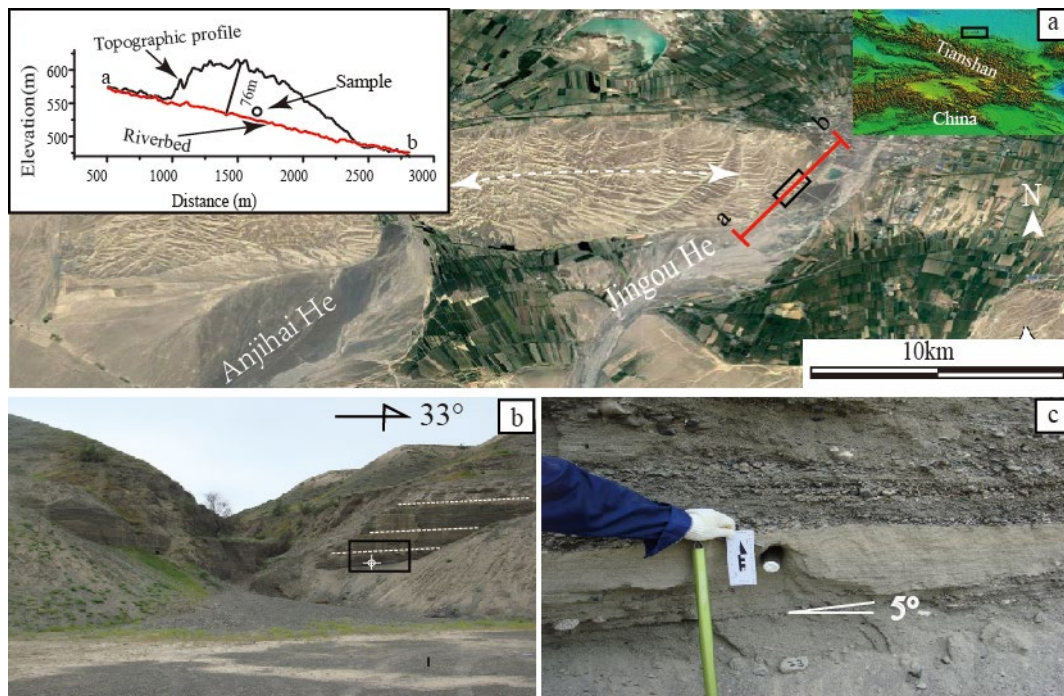
Fig. 1. *Sampling site at the eastern tip of Anjihai anticline and the lithology. a) Google Earth image of the Anjihai anticline. The black square marks the location of the strata for sampling. The inset is a topographic profile of the eastern tip Anjihai anticline with the sample location; photos shown in b) and c) are the close look of the sampling site and strata.*

300 ka due to dose saturation (Li and Li, 2012; Malatesta *et al.*, 2018), which might not be high enough for the strata presumed to be early Pleistocene. The multiple aliquots regenerative MET-pIRIR (MAR-MET-pIRIR) procedure helps double the characteristic saturation dose of MET-pIRIR signals and allows to date samples as old as 500 ka (Chen *et al.*, 2015), which makes it an ideal choice for dating old samples.

In this study, we are aiming to employ the state-of-art K-feldspar pIRIR and MET-pIRIR dating procedures to constrain the depositional age of the tectonically deformed fluvial sandy bed at the bottom of the outcrop on the eastern tip of Anjihai anticline. It is the first attempt of absolute dating, which is critical for the earthquake hazard evaluation for the cities nearby. The single grain K-feldspar pIRIR and MAR-MET-pIRIR procedures will be employed. For the single grain procedure, both the $pIRIR_{225}$ and $pIRIR_{290}$ signals are explored, taking consideration of their different stability and bleachability (Smedley *et al.*, 2015). Both the central age model (CAM) and minimum age model (MAM) are employed to derive the D_e values of the sample (Galbraith *et al.*, 1999). However, the application of MAM to pIRIR and MET-pIRIR D_e distributions may be biased to the grains with large fading rates rather than with well bleaching. Meanwhile, the mean and median D_e values are also calculated for comparison, upon which the depositional age of the tectonically deformed fluvial strata will be discussed.

2. SAMPLE, METHODS AND EXPERIMENTS

Sample

Previous studies have shown that the shortening rates of Anjihai anticline ranging from 0.5 mm/yr to 1.12 mm/yr during late Pleistocene, with luminescence ages available for its western tip (Deng *et al.*, 2000; Daëron *et al.*, 2007; Fu *et al.*, 2017; Lv *et al.*, 2017, 2019). If the depositional age of the sample from the eastern tip is not as old as early Pleistocene, it may suggest that the Anjihai anticline is active at both eastern and western tips, which is critical for seismic hazards evaluation. As that shown in **Fig. 1c**, the sample (JGH 18 OSL 23) was taken from a sandy lens with clear bedding and well sorting at the bottom of the loess and fluvial sedimentary sequence (with a thickness of 51m) at the eastern tip of Anjihai anticline. The bedding of the strata is slightly southward tilted due to tectonic deformation. The sample is 7.5m higher than the modern river bed.

Experimental details

The sample was prepared following the procedures of Aitken (1998). It was treated with HCl and H_2O_2 to remove the carbonates and organic matter, respectively, and then wet-sieved to separate grains in the size range of 125–180 µm. Subsequently, the K-feldspar grains

($\rho < 2.58$ g/cm^3) were enriched by density separation with the solution of lithium polytungstate. They were then subjected to HF (10%) etching for 40 min to remove the alpha particle irradiated layer and repeatedly rinsed by 10% HCl and distilled water to remove the fluorides.

For single grain measurements, the K-feldspar grains were mounted into the single grain disc with hole diameter of 200 µm and a depth of 200 µm. The single grain luminescence measurements were performed on an automated Risø DA-20 TL/OSL reader with dual – laser single grain attachment. The IR laser ($\lambda = 830$ nm, $P_{max} = 500$ mW/cm^2) with 90% of its full power was employed for IR stimulation, and the photon multiplier tube (PMT) of model 9235QB15 with blue filter pack (BG3 and BG39) mounted in front was used for detecting the blue emission from the K-feldspar grain. The dose rate of the $^{90}Sr/^{90}Y$ β irradiation source attached on the reader is 0.1852 ± 0.0044 Gy/s, calibrated using the single grain disc.

For the MAR-MET-pIRIR measurements, the K-feldspar grains were mounted on steel-stainless disc with silicon spray in diameters of 8 mm and 1 mm for large aliquot and small aliquot, respectively. The IR LEDs ($\lambda = 870$ nm, $P_{max} = 145$ mW/cm^2) with 90% of its full power was employed for all IR stimulations, and the PMT (model 9107QB70) with blue filter pack (BG3 and BG39) mounted in front was used for detecting the blue emission of the K-feldspar aliquots. The dose rate of the $^{90}Sr/^{90}Y$ β irradiation source attached on the reader is 0.2073 ± 0.0018 Gy/s, calibrated using the steel-stainless disc.

The radioactivity of the sample was measured with ORTEC GEM70P4-95 gamma spectrometry equipped with a Ge detector. The internal potassium concentration of K-feldspar grains was taken as 12.5% ± 0.5%. The dose rate of the sample was calculated by using the DRAC online calculator (Durcan *et al.*, 2015), with the water content estimated to be 10% ± 5%.

Methods

The $pIRIR_{225}$ (Buylaert *et al.*, 2009) and $pIRIR_{290}$ (Thiel *et al.*, 2011) signals are most frequently employed for dating old samples. The former one is bleached faster than the latter one, but suffers more anomalous fading. Therefore, they are both employed for the single grain procedure to determine the D_e value of individual K-feldspar grain (**Table 1**). For the recent application to the fluvial sediments, single grain $pIRIR_{225}$ signal is often adopted (Malatesta *et al.*, 2018; Kolb and Fuchs, 2018). There are two reasons for doing so. One is that the $pIRIR_{225}$ signal is easier to bleach than the $pIRIR_{290}$ signal (Buylaert *et al.*, 2012; Kars *et al.*, 2014), in particular for the water-lain sediments; the other is the potential initial sensitivity change induced by high-temperature treatment involved in the measurement of $pIRIR_{290}$ signal (Roberts, 2012; Qin *et al.*, 2018). The inheritance of thermally transferred pIRIR (TT-pIRIR) signal from natural and

Table 1. *Single-grain pIRIR and multiple-aliquot MET-pIRIR measurements procedures.*

Steps	Single grain pIRIR$_{225}$	Single grain pIRIR$_{290}$	MAR-MET-pIRIR$_{290}$
1	Natural or regenerative dose D$_i$	Natural or regenerative dose D$_i$	Natural or regenerative dose D$_i$
2	PH at 250°C for 60 s	PH at 320°C for 60 s	PH at 320°C for 60 s
3	IR laser @ 50°C for 1.2 s	IR laser @ 50°C for 1.2 s	IRLED @ 50°C for 100 s
4	IR laser @ 225°C for 1.2 s	IR laser @ 290°C for 1.2 s	IRLED @ 100°C for 100 s
5	IRLED @ 225°C for 100 s	IRLED @ 290°C for 100 s	IRLED @ 150°C for 100 s
6	Test dose	Test dose	IRLED @ 200°C for 100 s
7	PH at 250°C for 60 s	PH at 320°C for 60 s	IRLED @ 250°C for 100 s
8	IR laser @ 50°C for 1.2 s	IR laser @ 50°C for 1.2 s	IRLED @ 290°C for 100 s
9	IR laser @ 225°C for 1.2 s	IR laser @ 290°C for 1.2 s	Test dose
10	IRLED @ 290°C for 100 s	IRLED @ 325°C for 100 s	PH at 320°C for 60 s
11	Return to step1	Return to step1	IRLED @ 50°C for 100 s
12			IRLED @ 100°C for 100 s
13			IRLED @ 150°C for 100 s
14			IRLED @ 200°C for 100 s
15			IRLED @ 250°C for 100 s
16			IRLED @ 290°C for 100 s
17			**Solar simulator bleach for 4 hrs**
18			**Normalization dose D$_r$**
19			**Run steps 2-16**
20			Return to step1

1) For the natural sample, the given dose D$_i$ = 0 Gy
2) The same D$_r$ (D$_r$ = 518 Gy) is applied to procedure (c)

regenerative doses to pIRIR signals of the corresponding test dose may affect the dose response characteristics and the resultant D$_e$ values (Nian *et al.*, 2012; Qin and Zhou, 2012). In our experiment, the size of the test dose was optimised by making the ratio of TT-pIRIR signals of natural dose to the pIRIR signals of the following test dose be less than 15%. With consideration of the notorious initial sensitivity change of IRSL and pIRIR signal measurements (Wallinga *et al.*, 2000; Kars *et al.*, 2014; Colarossi *et al.*, 2018; Qin *et al.*, 2018; Zhang, 2018), the dose recovery experiment was employed to verify the measurement procedure by optimising the test dose.

The MAR-MET-pIRIR procedure of Li *et al.* (2017) was slightly modified to apply to the sample of this study. For the MAR-MET-pIRIR measurements, 8 mm large aliquots were bleached with SOL2 for 12 hours to remove the natural signal and given different regenerative doses ranging from ~310 Gy to ~1865 Gy to establish the dose response curve, and tens of 1 mm aliquots were prepared for measuring the natural MET-pIRIR signals. Six consecutive IR stimulation at progressively higher temperatures ranging from 50°C to 290°C were conducted after the preheat at 320°C for 60 s for both natural/regenerative and following test doses (**Table 1**). After measuring the sensitivity corrected MET-pIRIR signals of the natural (Ln/Tn) and regenerative doses (Lx/Tx), all 8 mm and 1 mm aliquots were subjected to 4 hrs SOL2 bleaching to remove the residual signals. Subsequently, the sensitivity corrected MET-pIRIR intensities of a common regenerative dose of 518 Gy (Lr/Tr) were measured to normalise the dose response variability among different aliquots.

Finally, the normalised Ln/Tn ((Ln/Tn)/(Lr/Tr)) values of 1 mm aliquots are projected onto the dose response curve established by the normalised Lx/Tx ((Lx/Tx)/(Lr/Tr)) of 8 mm aliquots to derive the D$_e$ values. Similar to the single grain procedure, the size of the test dose was also optimised to render the ratio of natural TT-MET-pIRIR to the MET-pIRIR intensity to be lower than 15%. To suppress the potential isothermal decay (Fu *et al.*, 2012) and photon transferred thermo-luminescence (PTTL, Qin *et al.*, 2015) contributions to the MET-pIRIR signals, the IR-off period increases from 10 s to 60 s with the increase of the stimulation temperatures.

In this study, we employed three criteria for screening the data for analysis: the recycling ratio is between 0.9 and 1.1, the integrated test dose pIRIR intensity is larger than 100 and higher than the 3σ of the background. The central age model (CAM) and minimum age model (MAM), as well as the mean and median, were applied to D$_e$ distributions determined by the single grain pIRIR and MAR-MET-pIRIR procedures, which were implemented in R package "Luminescence" (Dietze *et al.*,2015).

3. RESULTS

Luminescence characteristics

Decay curves

Single grain pIRIR and MAR-MET-pIRIR procedures were employed to obtain the D$_e$ distribution of the sample. For the single grain procedures, the pIRIR$_{225}$ and pIRIR$_{290}$ signals were measured following the procedures

shown in **Table 1a** and **1b**, which are slightly modified from the procedures of Buylaert *et al.* (2009) and Thiel *et al.* (2011), respectively. **Fig. 2a** and **2c** show the typical luminescence decay curves of pIRIR$_{225}$ and pIRIR$_{290}$ signals resulting from ~93 Gy β dose, respectively. They both decay to a constant level after 0.3s IR stimulation. The initial intensity of individual K-feldspar grain ranges from 500 to $1 \cdot 10^4$ and 600 to $8 \cdot 10^3$ for the pIRIR$_{225}$ and the pIRIR$_{290}$ signals, respectively, which are much higher than the background level at ~50 and ~70 respectively. The net intensity of single grain K-feldspar pIRIR signal was calculated as the integration of initial 0.04 s intensity of the decay curves with the subtraction of the integration of last 0.1 s intensity. For the MAR-MET-pIRIR procedure, the initial intensity of the decay curves of ~415 Gy β dose of 8 mm aliquot slightly increases with the stimulation temperature, except that of the MET-IR$_{50}$ signal (**Fig. 2e**). The initial 0.4 s was integrated as the signal, while the last 4.5 s was integrated as the background.

Thermal transfer

The inheritance of thermally transferred signals to the signals of the test dose is always concerned in the pIRIR measurements, which may lead to inappropriate sensitivity correction (Nian *et al.*, 2012; Qin and Zhou, 2012). The effect of thermally transferred signals could be largely suppressed by increasing the size of the test dose. In
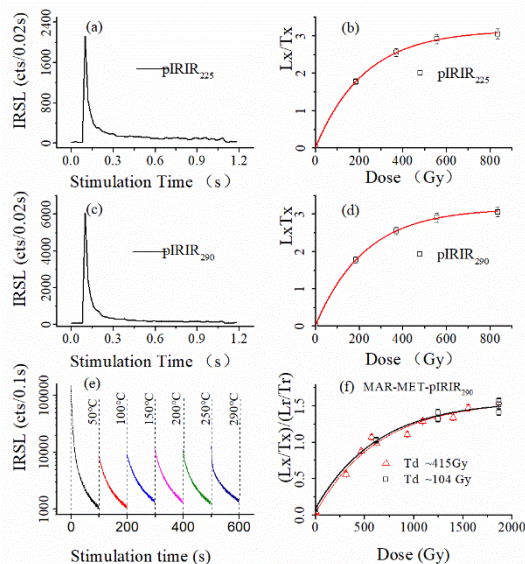
Fig. 2. *Typical luminescence decay curves and growth curves of the K-feldspar single grain pIRIR and MAR-MET-pIRIR signals. a) and b) are the decay curve and growth curve of single grain pIRIR$_{225}$ signal, respectively; c) and d) are the decay curve and growth curve of single grain pIRIR$_{290}$ signal, respectively; e) MAR-MET-pIRIR decay curves; f) typical growth curves of MAR-MET-pIRIR$_{290}$ signals. Black line\squares show the growth curve with a test dose of 104 Gy. Red line and triangles show the growth curve with a test dose of 415 Gy.*

this study, the ratio of thermally transferred signals of natural dose to the signal of the test dose to be less than 15% was taken as a criterion for optimising the test dose. After measuring the natural pIRIR signal of single grain or MET-pIRIR signals of 8 mm aliquot following the procedures shown in **Table 1**, the sample was preheated and stimulated again with no dose irradiation to measure the thermally transferred pIRIR (TT-pIRIR) and thermally transferred MET-pIRIR (TT-MET-pIRIR) signals. Subsequently, the pIRIR and MET-pIRIR responses to different test doses were measured. The same integration limits for the signal and background, as stated above, were taken for calculating the ratio of the TT-pIRIR (TT-MET-pIRIR) to the pIRIR (MET-pIRIR) signals. The frequency distribution in **Fig. 3a** and **3c** show that most of TT-pIRIR$_{225}$/pIRIR$_{225}$ and TT-pIRIR$_{290}$/pIRIR$_{290}$ ratio are 0.2 and 0.15, respectively, with the test dose of 31 Gy. By increasing the test dose to 93 Gy, such ratios decrease to less than 0.1 for both signals (**Fig. 3b** and **3d**). Therefore, the test dose was set to 93 Gy preliminarily for single grain measurements. Similar experiments were performed to evaluate the contribution of thermally transferred signals for the MAR-MET-pIRIR procedure shown in **Table 1** by using three 8 mm aliquots. **Fig. 4** shows the averaged TT-MET-pIRIR/MET-pIRIR ratios generally increase with the stimulation temperature. For stimulation temperatures ranging from 50°C to 250°C, such ratio is always less than 10% even the test dose is as low as 104 Gy. However, for the MET-pIRIR$_{290}$ signal, the ratio is as high as 30% with the test dose of 104 Gy. When the test dose increases to 415 Gy, such ratio decreases to ~15%. With the test dose further increased to 622 Gy, such ratio slightly decreases to ~11%.

Dose response

With the preliminarily chosen test dose, the single grain pIRIR and MAR-MET-pIRIR procedures shown in **Table 1** were employed to investigate the dose response characteristics. The saturating exponential equation was used to fit the dose response curves. Typical dose response curves (DRC) of single grain pIRIR$_{225}$ (**Fig. 2b**) and pIRIR$_{290}$ (**Fig. 2d**) signals show that these two signals are close to saturation with the regenerative dose of 800 Gy. However, the MAR-MET-pIRIR$_{290}$ DRC is not saturated until the regenerative dose is as large as 1866 Gy and the characteristic saturation dose (D_0) is 675 ± 35 Gy (**Fig. 2f**). In addition, the renormalised MAR-MET-pIRIR$_{290}$ DRC established by employing the test dose of 104 Gy is also shown in **Fig. 2f**, and it is not distinguished from the DRC with the test dose of 415 Gy.

Dose recovery test

The dose recovery test is a way to investigate whether the initial sensitivity change is significant for employing IRSL, pIRIR and MET-pIRIR signals from single aliquot for D$_e$ determination (Wallinga *et al.*, 2000; Kars *et al.*,
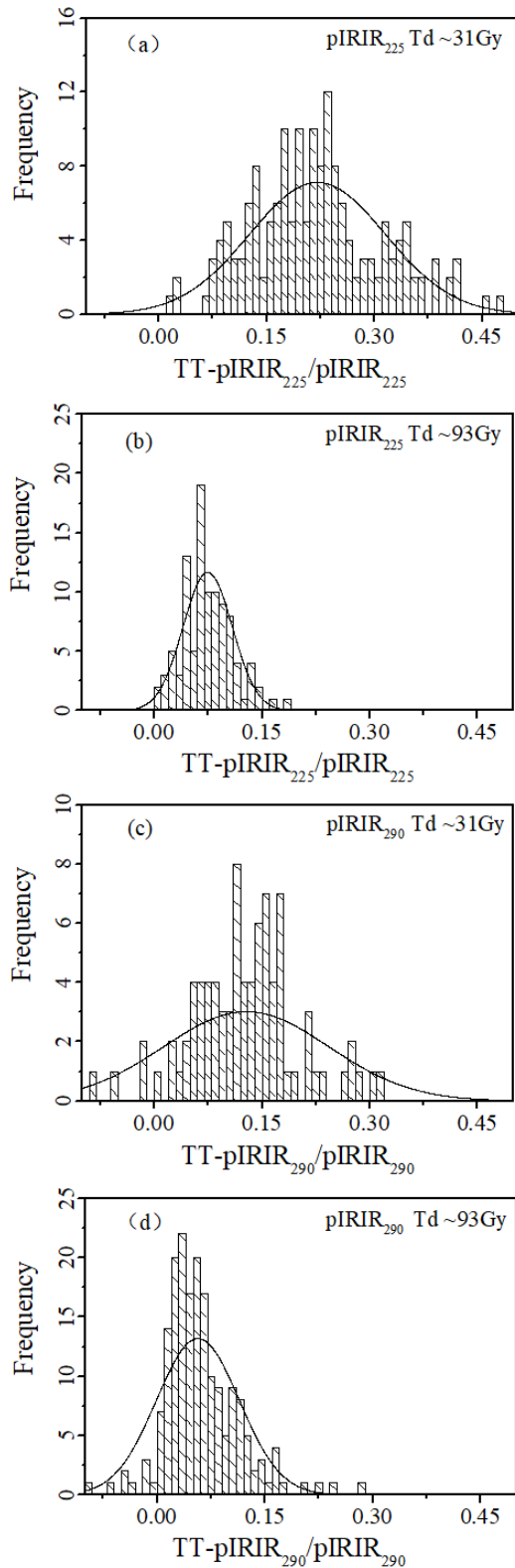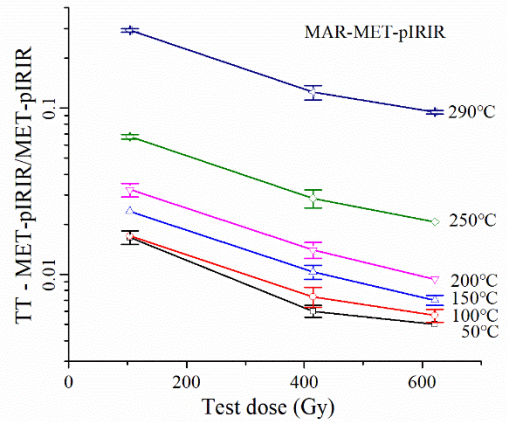
Fig. 4. *The dependence of thermal transfer ratios on the test dose. The thermal transfer ratio is evaluated with a test dose of ~103 Gy, ~415 Gy and ~622 Gy for MAR-MET-pIRIR signals, respectively.*
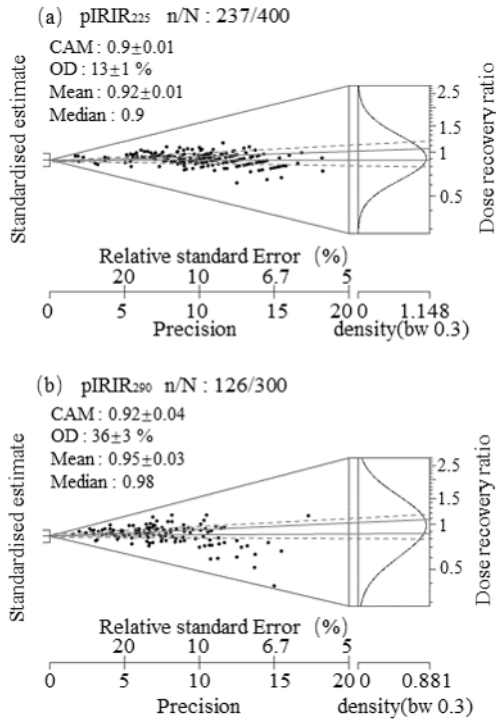
2014; Nian *et al.*, 2016; Yi *et al.*, 2016; Qin *et al.*, 2018). It would also apply to the single grain pIRIR measurements. Firstly, the K-feldspar grains were bleached by the solar simulator SOL2 for 12 hours to remove the natural signals. Then, 3000 s (in equivalence with 556 Gy) β irradiation was applied to the bleached grains. Subsequently, the single grain pIRIR measurement procedures (**Table 1a** and **1b**) were applied to the dosed K-feldspar grains with a test dose of 93 Gy. Since the given dose is fairly large in this study, the residual dose after 12 hours SOL2 bleaching is supposed to be negligible with respect to the reported residual $pIRIR_{225}$ and $pIRIR_{290}$ signals (Li and Li, 2011; Buylaert *et al.*, 2012; Rui *et al.*, 2015; Guo *et al.*,2015; Smedley *et al.*, 2015).

Fig. 5 shows dose recovery ratio (DRR) distribution for the single grain $pIRIR_{225}$ and $pIRIR_{290}$ measurements, respectively. The kernel density estimation (KDE) indicates the DRR distribution peaks around unity for both signals. The mean of DRR are 0.92 ± 0.01 and 0.95 ± 0.03 for the $pIRIR_{225}$ and $pIRIR_{290}$ signals, respectively. They are both in the acceptable range, although the DRRs are much more scattered for the $pIRIR_{290}$ signal. The over-dispersion (OD) determined by applying the central age model (CAM) to the dose recovery ratio distribution is $13\% \pm 1\%$ and $36\% \pm 3\%$ for the $pIRIR_{225}$ and $pIRIR_{290}$ signal, respectively.

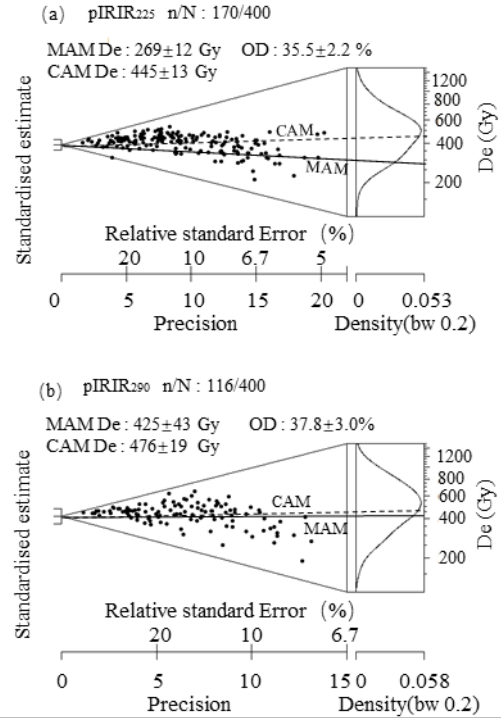### Equivalent dose determination

Single grain procedures

The single grain pIRIR procedures were applied to four hundred K-feldspar grains for both signals, and the data screening criteria was the same as those adopted for dose recovery test. 170 and 116 out of 400 grains were accepted for analysis for $pIRIR_{225}$ and $pIRIR_{290}$ signal, respectively, and the corresponding D_e distributions are shown by Abanico plots in **Fig. 6**. The CAM D_e are

Fig. 3. *The frequency distribution of thermal transfer ratios for single grain pIRIR$_{225}$ and pIRIR$_{290}$ signals with different test doses. a) and b) pIRIR$_{225}$ signal with a test dose of 31Gy and 93 Gy, respectively; c) and d) pIRIR$_{290}$ signal with a test dose 31 Gy and 93 Gy, respectively.*

Fig. 5. *The abanico plots of dose recovery results with a given dose of ~556 Gy and test dose ~93 Gy for single grain pIRIR225 and single grain pIRIR290 procedures. The solid line show the range between 0.9 and 1.1, while the dashed line show the range between 0.8 and 1.2.*

Fig. 6. *The abanico plot of D_e distribution for single grain pIRIR225 and single grain pIRIR290 procedures with a test dose of 93 Gy. MAM D_e was calculated with sigmab of 0.13 and 0.36 for pIRIR225 and pIRIR290 signals, respectively.*

445 ± 13 Gy and 476 ± 19 Gy for the pIRIR$_{225}$ and pIRIR$_{290}$ procedure, while the corresponding OD values are $35.5\% \pm 2.2\%$ and $37.8\% \pm 3.0\%$, respectively. The OD value of pIRIR$_{225}$ D_e is three times higher than the OD value of 13% determined by the dose recovery test, which may imply partial bleaching. However, for the pIRIR$_{290}$ signal, the OD of the D_e values is close to that of the dose recovery ratio, which is both around 36%. The minimum age model (MAM) was subsequently applied for the pIRIR$_{225}$ and pIRIR$_{290}$ D_e values, with the "σ_b" of 13% and 36% determined through the dose recovery test, respectively. The resultant MAM D_e are 269 ± 12 Gy and 425 ± 43 Gy for the pIRIR$_{225}$ and pIRIR$_{290}$ procedure,

respectively. The mean and median D_e are also calculated, and they are both close to the CAM D_e values for both signals (**Table 2**).

MAR-MET-pIRIR procedure

Fifty-six 1 mm aliquots were measured with the MAR-MET-pIRIR procedure shown in **Table 1**, and the normalised natural MET-pIRIR intensities were projected upon the DRCs established in Section 3 – Luminescence characteristics – Dose response to obtain D_e values. The KDE of MAR-MET-pIRIR$_{290}$ D_e values is shown in **Fig. 7a** as an example. The D_e values are rather dispersive, which range from 700 Gy to 2000 Gy, and the OD value

Table 2. *The statistics of D_e values.*

	Test dose (Gy)	MAM (Gy)	CAM (Gy)	Median (Gy)	Mean (Gy)	OD (%)	n/N[1]
SG pIRIR225	93	269±12	445±13	468	456	36±2	170/400
SG pIRIR290	93	425±43	476±19	500	496	38±3	116/400
MAR-pIRIR290[2]	104	762±40	872±21	888	886	15±2	59/60
MAR-pIRIR290[2]	415	811±44	977±27	968	1007	17±2	56/58

1) n is the number of K-feldspar grains or aliquots passing the rejection criteria and used for equivalent dose determination; N is total number of measured K-feldspar grains or aliquots.

2) Such pIRIR290 signals were measured with the multiple elevated temperature procedure.

is $17 \pm 2\%$. The OD values constrained for different stimulation temperatures range from 15% to 20%. Fu *et al.* (2015) reported an OD value of 10% for MET-pIRIR signals of loess samples from the same area. It implies that incomplete bleaching may contribute to the MAR-MET-pIRIR D_e distribution. Similar to the treatment for single grain D_e values, the CAM D_e, MAM D_e, median D_e and mean D_e values were calculated for the MET-pIRIR signals measured at different temperatures. The "σ_b" was taken as 10% for applying the MAM to all MAR-MET-pIRIR D_e values, which is based on the similar MET-pIRIR decay characteristics shown in **Fig. 2e**.

Fig. 8a shows the dependence of various statistics of D_e values on the stimulation temperatures. For each stimulation temperature, the D_e values resulted from different statistical methods are consistent, except that the MAM D_e is 100–150 Gy lower. Both CAM and MAM D_e increase with stimulation temperature in the range of 50°C to 250°C, and a plateau is observed between 250°C and 290°C, which implies that the CAM and MAM D_e values in this range are not affected by anomalous fading (Li and Li, 2011). Since the D_e values are as large as 800 Gy, the characteristic saturation doses (D_o) of MAR-MET-pIRIR dose response curves are closely examined. The D_o value decreases from 829 ± 127 Gy to 644 ± 76 Gy with the increase of stimulation temperature in general (**Fig. 8a**).

MAR-MET-pIRIR D_e values determined with a test dose of 104 Gy are compared. **Fig. 7b** shows that the MAR-MET-pIRIR$_{290}$ D_e values range from 520 Gy to 1300 Gy. A plateau was also identified between 250°C

and 290°C. The large test dose of 415 Gy resulted in slightly larger MAM and CAM D_e values than those obtained with the test dose of 104 Gy, while the median and KDE peak of the D_e distribution are close to those with the test dose of 104 Gy (**Fig. 7a**). With the test dose of 415 Gy and 104 Gy, the MAM D_e are 811 ± 44 Gy and 762 ± 40 Gy, while the CAM D_e are 977 ± 27 Gy and 872 ± 21 Gy, respectively. The median and mean D_e values are consistent with CAM D_e values for both procedures. Such differences in D_e values between these two procedures with different test doses suggest that the thermal transfer may lead to slight underestimation (7%–10%) of D_e values.

4. DISCUSSION

Methodological uncertainties

Although the K-feldspar pIRIR or MET-pIRIR signals are of potential to date the water-lain sediments beyond late-Pleistocene, challenges arise both internally and externally, which include (1) the inheritance of pIRIR signals due to thermal transfer effect (Nian *et al.*, 2012; Qin and Zhou, 2012); (2) the initial sensitivity change due to high temperature heating (Wallinga *et al.*, 2000; Roberts, 2012; Kars *et al.*, 2014; Qin *et al.*, 2018); (3) the variability of anomalous fading among grains (Reimann

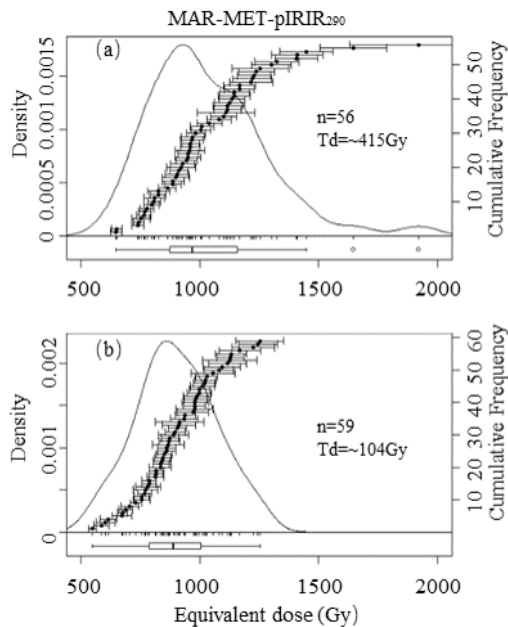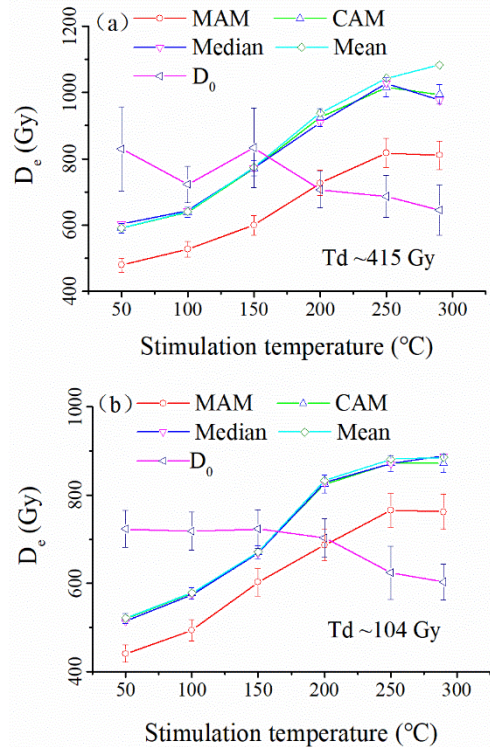**Fig. 7.** *Kernel density estimate of MAR-MET-pIRIR$_{290}$ D_e values. D_e distributions measured with test dose of ~415 Gy and ~104 Gy are shown in a) and b), respectively.*

Fig. 8. *Dependence of MAR-MET-pIRIR D_e values on stimulation temperature. a) with a test dose of 415 Gy; b) with a test dose of 104 Gy.*

et al., 2012; Kars *et al.*, 2014; Rui *et al.*, 2019); (4) the slow bleaching characteristic of high temperature pIRIR and MET-pIRIR signals (Buylaert *et al.*, 2012; Li *et al.*, 2014). In this study, these complexities were treated carefully.

The effect of thermally transferred pIRIR and MET-pIRIR signals were suppressed by increasing the size of the test dose. The test dose was optimised to be ~20% to ~40% of the CAM D_e for the single grain pIRIR and MAR-MET-pIRIR procedures, respectively, which made the contribution of thermally transferred signals to the corresponding pIRIR and MET-pIRIR signals to be less than 15% (**Fig. 3** and **Fig. 4**). It is just from the aspect of suppressing the thermal transfer. However, the size of test dose is also subtle for recovering a known dose irradiated in the laboratory by the single aliquot or single grain pIRIR and MET-pIRIR procedures (Nian *et al.*, 2016; Yi *et al.*, 2016; Qin *et al.*, 2018), which is an indicator of any initial sensitivity change (Kars *et al.*, 2014; Qin *et al.*, 2018). The dose recovery experiments performed for the single grain pIRIR procedures validated the choice of test dose on the basis of averaged behaviour of K-feldspar grains. However, the DRR values are rather scattered, especially for the pIRIR$_{290}$ signal (**Fig. 5**). Further, the appropriateness of the size of test dose depends significantly on the size of natural or given dose (Yi *et al.*, 2016; Qin *et al.*, 2018); therefore, a common test dose may not be appropriate for K-feldspar grains with a wide distribution of D_e values shown in **Fig. 6**. It implies that the uncertainties arising from varying initial sensitivity change among K-feldspar grains may contribute to the observed dispersion of single grain pIRIR D_e values, for which further investigations are still needed. Since the aliquots are not heated prior to the irradiation of natural or regenerative dose, the MAR-MET-pIRIR procedure is expected to be less affected by initial sensitivity changes if such changes are the same from the natural dose and regenerative dose to their corresponding test dose, respectively (Li *et al.*, 2017; Qin *et al.*, 2018).

Since the sample is water-lain, the potential incomplete bleaching evidenced by large OD of single grain pIRIR D_e value necessitates the implementation of the MAM. The rationale for implementing the MAM is that the scatter in single grain D_e values is mainly due to different bleaching extents of pIRIR signal of K-feldspar grains before deposition. However, the anomalous fading also varies among grains, and it is difficult to measure the fading rate on individual grain level. Therefore, there is a potential risk of biasing to grains with more fading rather than sufficient bleaching when implementing the MAM. As an alternative, the pIRIR sensitivity is a possible index for anomalous fading of K-feldspar grains (Smedley *et al.*, 2015; Reimann *et al.*, 2012; Rhodes, 2015). Although a weak positive correlation is observed between the natural log of pIRIR$_{290}$ sensitivities and D_e values for K-feldspar grains of this study (**Fig. 9a**, the slope of linear regression is 18.8 with the Pearson R of 0.05), the

scatter of D_e values decreases with the pIRIR sensitivity. A more significant positive correlation between these two quantities is observed for the pIRIR$_{225}$ signal (**Fig. 9c**, the slope of linear regression is 87.2 with the Pearson R of 0.24). **Fig. 9b** and **9d** show that the CAM D_e values for the brightest K-feldspar grains (pIRIR intensity larger than 10^4) are ~550 Gy for both the pIRIR$_{225}$ and pIRIR$_{290}$ signals. Malatesta *et al.* (2018) employed the OD values calculated after pIRIR sensitivity screening to identify the well bleached grains and still applied the fading correction to the brightest K-feldspar grains. In this study, the OD values decrease from 36% to 20% with the increase of pIRIR sensitivity employed for screening and may imply better bleaching for K-feldspar grains with high pIRIR sensitivity.

Comparison among various procedures

The D_e distributions determined by different procedures are shown in **Fig. 10**. Except for the MAM D_e of the single grain pIRIR$_{225}$ signal, other statistical metrics cluster around 455 Gy and 490 Gy for the single grain pIRIR$_{225}$ and pIRIR$_{290}$ procedure, respectively (**Table 2**), although the variation is much larger for the former (grey shaded area). However, they are consistently lower than the MAR-MET-pIRIR$_{290}$ D_e values. The MAM MAR-MET-pIRIR$_{290}$ D_e of 811 ± 44 Gy is 1.9 times and three times higher than the single grain MAM pIRIR$_{290}$ and MAM pIRIR$_{225}$ D_e, respectively, which might be partly attributed to the anomalous fading of the single grain pIRIR signals. Malatesta *et al.* (2018) employed an averaged fading rate of 4.32 ± 0.38% to correct the fading of pIRIR$_{225}$ signals of their K-feldspar grains taken from the
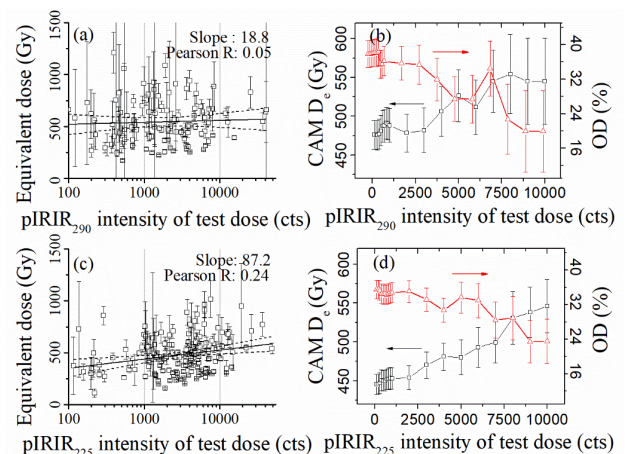
Fig. 9. *Dependence of K-feldspar single grain D_e value on the pIRIR sensitivity (response to a test dose of 93 Gy) a) pIRIR$_{225}$ and c) pIRIR$_{290}$ signals. The solid line is linear fit and the dashed line is the 95% confidence band. The dependence of CAM D_e and OD on the lowest pIRIR sensitivity employed to screen the K-feldspar for analysis are shown in b) and d).*
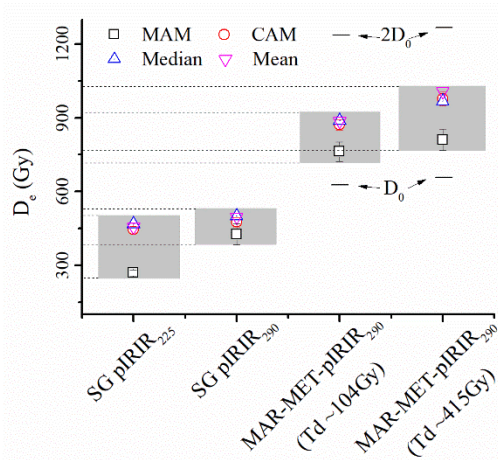
Fig. 10. *Comparison of D_e values obtained by the single grain pIRIR procedures and MAR-MET-pIRIR$_{290}$ procedures. Various statistical models were applied to the measured D_e values. The D_0 and $2 \cdot D_0$ values are shown for MAR-MET-pIRIR$_{290}$ procedures with test doses of 104 Gy and 415 Gy, respectively. The shaded region shows the whole range of D_e values measured with different procedures.*

same area, and it led to 46%–70% increase in D_e values for their samples with uncorrected D_e values close to our study (**Table 2** of the supplementary material of Malatesta *et al.*, 2018). If such correction were applied to the sample of this study, the corrected D_e would be 803 to 935 Gy, which are more or less close to the MAR-MET-pIRIR$_{290}$ D_e value. Apart from the anomalous fading, the inaccurate sensitivity correction may also contribute to the systematic D_e discrepancy between single grain pIRIR and MAR-MET-pIRIR$_{290}$ signals (Li *et al.*, 2013a; Chen *et al.*, 2015), for which further investigations are still needed.

The characteristic saturation dose (D_o) is of concern when an old sample is dated. The D_o value of the MET-MAR-pIRIR$_{290}$ signals are 644 ± 76 Gy and 603 ± 41 Gy with the test dose of 415 Gy and 104 Gy, respectively (**Fig. 10**). Even the largest D_e value (upper dashed line of the grey shaded area) is much smaller than the $2 \cdot D_o$. Therefore, the MAR-MET-pIRIR$_{290}$ D_e values are in the range of theoretical upper dating limit.

Preliminary ages and geological implication

With consideration of various uncertainties associated with different measurement procedures, the MAM D_e of 811 ± 44 Gy determined by using the MAR-MET-pIRIR$_{290}$ procedure with the test dose of 415 Gy is the most reliable for the fluvial silt of this study. The concentration of uranium, radium, thorium and potassium measured by using the gamma spectrometry equipped with Ge

detector is 16.25 ± 4.62 Bq/kg, 9.90 ± 0.30 Bq/kg, 19.32 ± 0.30 Bq/kg and 593.33 ± 10.01 Bq/kg. The internal potassium content and water content are estimated to be $12.5 \pm 0.5\%$ and $10 \pm 5\%$, respectively. The resultant dose rate for the 125–180 μm K-feldspar grains is 2.85 ± 0.85 Gy/ka, and the burial age determined for this fluvial silt sample is 284 ± 86 ka. This age is much younger than the early Pleistocene epoch assigned to the fluvial strata before (Deng *et al.*, 2000). Therefore, the resultant rate of tilting and shortening would be twice at least, which may imply more active tectonics than previously inferred for the study area.

5. CONCLUSIONS

In this study, multi-methods luminescence dating was applied to a fluvial silt sample taken from the sandy bed of the basal deformed fluvial strata at the eastern tip of Anjihai anticline on the northern piedmont of Tian Shan. The single grain pIRIR and MAR-MET-pIRIR procedures were optimised with consideration of the methodological uncertainties such as thermal transfer and initial sensitivity change. The central age model and minimum age model were applied to the D_e distribution determined by the single grain pIRIR$_{225}$, single grain pIRIR$_{290}$ and MAR-MET-pIRIR$_{290}$ signals. The MAM D_e values are 11%–17% lower than the CAM D_e values except for the single grain pIRIR$_{225}$ procedure. The MAM D_e values determined by the single grain pIRIR procedures are underestimated by more than 40% when compared with the MAM D_e of MAR-MET-pIRIR$_{290}$ procedure, which might be attributed to the uncorrected fading of single grain pIRIR measurements. The MAR-MET-pIRIR procedure, which suffers less from the initial sensitivity change and enables the stable signal to be isolated, gives the more reliable D_e value for the sandy fluvial sample of this study. The MAM MAR-MET-pIRIR$_{290}$ D_e of 811 ± 44 Gy results in a burial age of 284 ka, which is much younger than that inferred previously and may imply a more active folding of the eastern tip of Anjihai anticline.

REFERENCES

Aitken MJ, 1998. *An Introduction to Optical Dating*. Oxford University Press, Oxford.

Avouac JP, Tapponnier P, Bai M, You H and Wang G, 1993. Active thrusting and folding along the Northern Tien Shan and late Cenozoic rotation of the traim relative to Dzungaria and Kazakhstan. *Journal of Geophysical research* 98: 6755–6804.

Brill D, Reimann T, Wallinga J, May SM, Engel M, Riedesel S and Brückner H, 2018. Testing the accuracy of feldspar single grains to date late Holocene cyclone and tsunami deposits. *Quaternary Geochronology* 48: 91–103, DOI 10.1016/j.quageo.2018.09.001.

Brown ND, Rhodes EJ, Antinao JL and McDonald EV, 2015. Single-grain post-IR IRSL signals of K-feldspars from alluvial fan deposits in Baja California Sur, Mexico. *Quaternary International* 362: 132–138, DOI 10.1016/j.quaint.2014.10.024.

Buylaert JP, Murray AS, Thomsen KJ and Jain M, 2009. Testing the potential of an elevated temperature IRSL signal from K-feldspar. *Radiation Measurements* 44: 560–565, DOI 10.1016/j.radmeas.2009.02.007.

Buylaert JP, Thiel C, Murray AS, Vandenberghe DAG, Yi SW and Lu HY, 2011. IRSL and post-IR IRSL residual doses recorded in modern dust samples from the Chinese Loess Plateau. *Geochronometria* 38(4): 432–440, DOI 10.2478/s13386-011-0047-0.

Buylaert JP, Jain M, Murray AS, Thomsen KJ, Thiel, C and Sohbati R, 2012. A robust feldspar luminescence dating method for Middle and Late Pleistocene sediments. *Boreas* 41: 435–451, DOI 10.1111/j.1502-3885.2012.00248.x.

Chen YW, Li SH, Li B, Hao QZ and Sun J, 2015. Maximum age limitation in luminescence dating of Chinese loess using the multiple-aliquot MET-pIRIR signals from K-feldspar. *Quaternary Geochronology* 30: 207–212, DOI 10.1016/j.quageo.2015.01.002.

Colarossi D, Duller GAT, Roberts HM, Tooth S and Lyons R, 2015. Comparison of paired quartz OSL and feldspar post-IR IRSL dose distributions in poorly bleached fluvial sediments from South Africa. *Quaternary Geochronology* 30(B): 233–238, DOI 10.1016/j.quageo.2015.02.015.

Colarossi D, Duller GAT and Roberts HM, 2018. Exploring the behaviour of luminescence signals from feldspars: Implications for the single aliquot regenerative dose protocol. *Radiation Measurements* 109: 35–44, DOI 10.1016/j.radmeas.2017.07.005.

Daëron M, JP Avouac and Charreau J, 2007. Modeling the shortening history of a fault tip fold using structural and geomorphic records of deformation. *Journal of Geophysical Research* 112: B03S13, DOI 10.1029/2006JB004460.

Deng QD, Feng XY, Zhang PZ, Xu XW, Yang XP, Peng SZ and Li J, 2000. *Tianshan Activity Structure*. Earthquake Press, China.

Deng QD, Feng XY, Zhang PZ, Xu XW, Ynag XP, Pen SZ and Li J, 2013. *The geology map of thrust-and-fold belt of northern Tianshan, China.* Earthquake Press, China.

Dietze M, Kreutzer S, Burow C, Fuchs MC, Fischer M and Schmidt C, 2015. The abanico plot: visualising chronometric data with individual standard errors. *Quaternary Geochronology* 31: 12–18, DOI 10.1016/j.quageo.2015.09.003.

Durcan JA, King GE and Duller GAT, 2015. DRAC: Dose Rate and Age Calculator for trapped charge dating. *Quaternary Geochronology* 28: 54–61, DOI 10.1016/j.quageo.2015.03.012.

Fu X, Li B and Li SH, 2012. Testing a multi-step post-IR IRSL dating method using polymineral fine grains from Chinese loess. *Quaternary Geochronology* 10: 8–15, DOI 10.1016/j.quageo.2011.12.004.

Fu X, Li SH, Li B and Fu BH, 2017. A fluvial terrace record of late Quaternary folding rate of the Anjihai anticline in the northern piedmont of Tian Shan, China. *Geomorphology* 278: 91–104, DOI 10.1016/j.geomorph.2016.10.034.

Fu X, Li SH and Li B, 2015. Optical dating of aeolian and fluvial sediments in north Tian Shan range, China: Luminescence characteristics and methodological aspects. *Quaternary Geochronology* 30: 161–167, DOI 10.1016/j.quageo.2015.03.001.

Guo YJ, Li B, Zhang JF and Roberts RG, 2015. Luminescence-based chronologies for Palaeolithic sites in the Nihewan basin, northern China: First tests using newly developed optical dating procedures for potassium feldspar grains. *Journal of Archaeological Science: Reports* 3: 31–40, DOI 10.1016/j.jasrep.2015.05.017.

Galbraith RF, Roberts RG, Laslett GM, Yoshida H and Olley JM, 1999. Optical dating of single and multiple grains of quartz from jinmium rock shelter, northern australia: part 1, experimental design and statistical models. *Archaeometry* 41: 339–364, DOI 10.1111/j.1475-4754.1999.tb00987.x.

Kars RH, Reimann T, Ankjaergaard C and Wallinga J, 2014. Bleaching of the post- IR IRSL signal: new insights for feldspar luminescence dating. *Boreas* 43: 780–791, DOI 10.1111/bor.12082.

Kolb T and Fuchs M, 2018. Luminescence dating of pre-Eemian (pre-MIS 5e) fluvial terraces in Northern Bavaria (Germany) – Benefits and limitations of applying a pIRIR$_{225}$-approach. *Geomorphology* 321: 16–32, DOI 10.1016/j.geomorph.2018.08.009.

Li B, Jacobs Z and Roberts RG, 2017. An improved multiple-aliquot regenerative-dose (MAR) procedure for post-IR IRSL dating of K-feldspar. *Ancient TL* 35: 1–8.

Li B, Jacobs Z, Roberts RG and Li SH, 2013a. Extending the age limit of luminescence dating using the dose-dependent sensitivity of MET-pIRIR signals from K-feldspar. *Quaternary Geochronology* 17: 55–67, DOI 10.1016/j.quageo.2013.02.003.

Li B, Jacobs Z, and Li SH, 2018. Single-grain dating of potassium-rich feldspar grains: Towards a global standardised growth curve for the post-IR IRSL signal. *Quaternary Geochronology* 45: 23–36, DOI 10.1016/j.quageo.2018.02.001.

Li B and Li SH, 2011. Luminescence dating of K-feldspar from sediments: a protocol without anomalous fading correction. *Quaternary Geochronology* 6: 468–479, DOI 10.1016/j.quageo.2011.05.001.

Li B and Li SH, 2012. Luminescence dating of Chinese loess beyond 130 ka using the non-fading signal from K-feldspar. *Quaternary Geochronology* 10: 24–31, DOI 10.1016/j.quageo.2011.12.005.

Li B, Roberts RG, Jacobs Z and Li SH, 2014. A single-aliquot luminescence dating procedure for K-feldspar based on the dose-dependent MET-pIRIR signal sensitivity. *Quaternary Geochronology* 20: 51–64, DOI 10.1016/j.quageo.2013.11.001.

Li T, J Chen, JA Thompson, Burbank DW and Yang XD, 2013b. Quantification of three-dimensional folding using fluvial terraces: A case study from the Mushi anticline, northern margin of the Chinese Pamir. *Journal of Geophysical Research – Solid Earth* 118: 4628–4647, DOI 10.1002/jgrb.50316.

Lv HH, Li BJ, Wu DY, Zhao JX, Zheng XM, Xiong JG and Li YL, 2019. Spatiotemporal patterns of the Late Quaternary deformation across the northern Chinese Tian Shan foreland. *Earth-Science Reviews* 194: 19–37, DOI 10.1016/j.earscirev.2019.04.026.

Lv HH, Wu DY, Cheng L, Zhang TQ, Xiong JG, Zheng XM and Li YL, 2017. Late Quaternary drainage evolution in response to fold growth in the northern Chinese Tian Shan foreland. *Geomorphology* 299: 12–23, DOI 10.1016/j.geomorph.2017.09.037.

Malatesta LC, Avouac JP, Brown ND, Breitenbach SFM, Pan JW, Chevalier ML, Rhodes E, Dimitri SC, Zhang WJ, Charreau J, Lave J and Blard PH, 2018. Lag and mixing during sediment transfer across the Tian Shan piedmont caused by climate-driven aggradation-incision cycles. *Basin Research* 30(4): 613–635, DOI 10.1111/bre.12267.

Nian XM, Bailey RM and Zhou LP, 2012. Investigations of the post-IR IRSL protocol applied to single K-feldspar grains from fluvial sediment samples. *Radiation Measurements* 47: 703–709, DOI 10.1016/j.radmeas.2012.03.024.

Nian XM, Li F, Chen FY, Zhang WG, Zhao YC, Zhou J and Gao X, 2016. Optically stimulated luminescence ages for human occupation during the penultimate glaciation in the western Loess Plateau of China. *Journal of Quaternary Science* 31: 928–935, DOI 10.1002/jqs.2917.

Qin JT, Chen J, Li YT and Zhou LP, 2018. Initial sensitivity change of K-feldspar pIRIR signals due to uncompensated decrease in electron trapping probability: Evidence from radiofluorescence measurements. *Radiation Measurements* 120: 131–136, DOI 10.1016/j.radmeas.2018.06.017.

Qin JT, Chen J and Salisbury JB, 2015. Photon transferred TL signals from potassium feldspars and their effects on post-IR IRSL measurements. *Journal of Luminescence* 160: 1–8, DOI 10.1016/j.jlumin.2014.11.022.

Qin JT and Zhou LP, 2012. Effects of thermally transferred signals in the post-IR IRSL SAR protocol. *Radiation Measurements* 47: 710–715, DOI 10.1016/j.radmeas.2011.12.011.

Reimann T, Thomsen KJ, Jain M, Murray AS and Frechen M, 2012. Single-grain dating of young sediments using the pIRIR signal from feldspar. *Quaternary Geochronology* 11: 28–41, DOI 10.1016/j.quageo.2012.04.016.

Rhodes EJ, 2015. Dating sediments using potassium feldspar single-grain IRSL: Initial methodological considerations. *Quaternary International* 362: 14–22, DOI 10.1016/j.quaint.2014.12.012.

Roberts HM, 2012. Testing Post-IR IRSL protocols for minimising fading in feldspars using Alaskan loess with independent chronological control. *Radiation Measurements* 47: 716–724, DOI 10.1016/j.radmeas.2012.03.022.

Rui X, Guo YJ, Zhang JF, Hu Y, Mei HJ, Wang YP, Xie F and Li B, 2019. Luminescence chronology of the Palaeolithic–Neolithic transition in the Yujiagou site at the Nihewan Basin, northern China. *Journal of Quaternary Science* 34: 125–137, DOI 10.1002/jqs.3086.

Rui X, Zhang JF, Hou YM, Yang ZM, Liu Y, Zhen ZM and Zhou LP, 2015. Feldspar multi-elevated-temperature post-IR IRSL dating of the Wulanmulun Palaeolithic site and its implication. *Quaternary Geochronology* 30: 438–444, DOI 10.1016/j.quageo.2015.05.004.

Smedley RK, Duller GAT, Roberts HM, 2015. Bleaching of the post-IR IRSL signal from individual grains of K-feldspar: implications for single-grain dating. *Radiation Measurements* 79: 33–42, DOI 10.1016/j.radmeas.2015.06.003.

Thiel C, Buylaert JP, Murray A, Terhorst B, Hofer I, Tsukamoto S and Frechen M, 2011. Luminescence dating of the stratzing loess profile (Austria) - testing the potential of an elevated temperature post-IR IRSL protocol. *Quaternary International* 234: 23–31, DOI 10.1016/j.quaint.2010.05.018.

Thomsen KJ, Murray AS, Jain M and Bøtter-Jensen L, 2008. Laboratory fading rates of various luminescence signals from feldspar-rich sediment extracts. *Radiation Measurements* 43: 1474–1486, DOI 10.1016/j.radmeas.2008.06.002.

Wallinga J, Murray A and Duller G, 2000. Underestimation of equivalent dose in single-aliquot optical dating of feldspars caused by preheating. *Radiation Measurements* 32: 691–695, DOI 10.1016/S1350-4487(00)00127-X.

Yi SW, Buylaert JP, Murray AS, Lu HY, Thiel C and Lin Z, 2016. A detailed post-IR IRSL dating study of the Niuyangzigou loess site in northeastern China. *Boreas* 45: 644–657, DOI 10.1111/bor.12185.

Zhang JJ, 2018. Behavior of the electron trapping probability change in IRSL dating of K-feldspar: A dose recovery study. *Quaternary Geochronology* 44: 38–46, DOI 10.1016/j.quageo.2017.12.001.